Eur. Phys. J. D **40**, 115–123 (2006)
DOI: 10.1140/epjd/e2006-00128-9

THE EUROPEAN PHYSICAL JOURNAL D

Melting, freezing and nucleation in nanoclusters of potassium chloride

I - Molecular dynamics simulation

P.C.R. Rodrigues and F.M.S. Silva Fernandes[a]

Department of Chemistry and Biochemistry, Faculty of Sciences, University of Lisboa, Campo Grande, Bloco C8, 1749-016 Lisboa, Portugal

Received 13 March 2006 / Received in final form 21 April 2006
Published online 15 June 2006

Abstract. Molecular dynamics simulations of the melting, freezing and nucleation are presented for unconstrained nanoclusters of KCl with a number of ions between 512 and 10648. The maximum extent of the probed liquid supercooling is analysed to the light of theoretical predictions and compared with experimental data. The fraction of the solid-like ions in the supercooled liquid is used as an indicator of heterogeneities within the liquid. Induced nucleation by seeding the supercooled liquid indicates that solid-liquid coexistence is stable, and sustained during the lifetime of the clusters, relatively to the supercooled liquid. A phenomenological analysis on the relaxation times of the crystal growth process is made. Critical nuclei sizes computed from the effectiveness of the seeds in the heterogeneous nucleation of the supercooled liquid, and from the residual crystallites in clusters not totally melted, are presented as a function of the temperature. The behavior of the systems is followed through various properties such as liquid and solid molar fractions, enthalpies of melting, heat capacities, self-diffusion coefficients and relaxation times related to the freezing process. The consistency of the simulation results for the heterogeneous nucleation is assessed by means of a classical nucleation model, from which an estimate of the interfacial surface tension is also worked out and compared with experimental data.

PACS. 61.46.-w Nanoscale materials: clusters, nanoparticles, nanotubes, and nanocrystals – 64.70.Nd Structural transitions in nanoscale materials

1 Introduction

Clusters have motivated a growing interest due to the theoretical challenges and the contributions of their study to other fields such as nucleation and crystal growth, structure of amorphous materials, catalysis and atmospheric chemistry. The study of phase transitions is of the utmost importance regarding a comparative behaviour in such small systems and in the bulk [1–17].

The actual technology opened the way to obtain a significant amount of experimental data [18–23], some taken at the atomic level [24] and even covering phase change processes [25,26]. Cluster crystallography data is also presented in the literature [27]. The importance of clusters in nucleation and crystal growth has been discussed by some authors [28–30].

Several workers [3,8,31–48] have performed simulations on unconstrained clusters that provide evidence of (i) first-order phase transitions and solid-liquid coexistence in single clusters; (ii) pronounced hysteresis cycles; (iii) glass-like transitions by instantaneously cooling the liquid and (iv) crystal-defective growth for the largest clusters by slowly cooling the liquid. In a previous work [45] we have reported an extensive simulation of the melting, for KCl and LiCl clusters, showing, in particular, that for sizes below 512 ions phase coexistence is practically absent. However, clusters whose sizes are over 512 ions present solid-liquid coexistence in a progressively large extent asymptotically approaching a phase change at constant temperature as the size increases.

The main objective of the present work is to extend our previous studies to the freezing process and to analyse the stability of the solid-liquid coexistence relatively to the supercooled liquid, by simulating homogeneous and heterogeneous nucleation in KCl nanoclusters of different sizes for relaxation times of the order of 10^2 ns. The consistency of the simulation results concerned with heterogeneous nucleation is assessed by means of a classical nucleation model. Furthermore the whole set of simulation results and the phenomenological analysis presented pave the way to a theoretical model for the coexistence of solid and liquid phases in finite systems, to be reported in a forthcoming paper [49].

The computational details are given in the following section. The melting and freezing processes are detailed

[a] e-mail: fsilva@fc.ul.pt

and discussed in Sections 3 and 4. Section 5 contains the concluding remarks.

2 Computational details

The molecular dynamics computations have been performed using the Born-Mayer-Huggins potential:

$$\phi_{ij}(r) = \frac{z_i z_j e^2}{r} + c_{ij} b \exp\left[\frac{\sigma_{ij} - r}{d}\right] - \frac{C_{ij}}{r^6} - \frac{D_{ij}}{r^8} \quad (1)$$

with the parameters given by Watts and McGee [50]. Verlet's leapfrog algorithm [51] for the numerical integration of Newton's equations of motion, with a time step of 5×10^{-15} s, has been used in all simulations. It is well-known that this potential, despite being a rigid-ion effective potential, reproduces some bulk properties of alkali halides and other substance [52–57].

Thermal properties have been calculated with a number of steps in the range 10^5–10^8, depending on the size of the clusters and the phase transition region. Thus, the longer runs correspond to time scales of the order of 10^2 ns. The determination of the velocity auto-correlation functions has been based on runs of 1.6×10^4–4×10^6 time steps with a time origin at every fifth step. As the clusters are unconstrained, the pressure is virtually zero.

The calculation of each state point has been carried out by fixing the total energy of the system and determining the corresponding average temperature (through the energy equipartition theorem [58]), instead of fixing a preset average temperature and calculating the resulting average total energy. This is a noteworthy detail referred to elsewhere [45]. We should point out, however, that there is nothing unusual or special in conducting constant-energy instead of constant-temperature simulations. Both approaches produce, of course, equivalent results for homogeneous phases. They are also able to detect phase transition regions in clusters. Nonetheless, it turns out that constant-energy simulations are more suitable to unravel some important properties of phase changes in clusters, which otherwise may remain hidden. For example, the assessment of the molar fractions of the coexistent phases. Incidentally, the method of fixing the total energy of clusters was used, for instance, by Briant and Burton [2] many years ago and, more recently, by Cleveland et al. [42].

For the freezing process we have used three distinct starting points: (a) a totally melted configuration; (b) a configuration not completely melted containing residual crystallites and (c) a supercooled liquid configuration plus a solid seed. The starting points for the solid phases have been f.c.c (rock salt) lattices at 0 K.

Heating/cooling rates in the range 0.3–377 $\times$ 10^9 kJ mol^{-1} s^{-1} ($\sim 10^{10}$–10^{13} K s^{-1}) have been used. These rates were chosen in order to maintain the system as close to equilibrium as possible within the limits of computational expense.

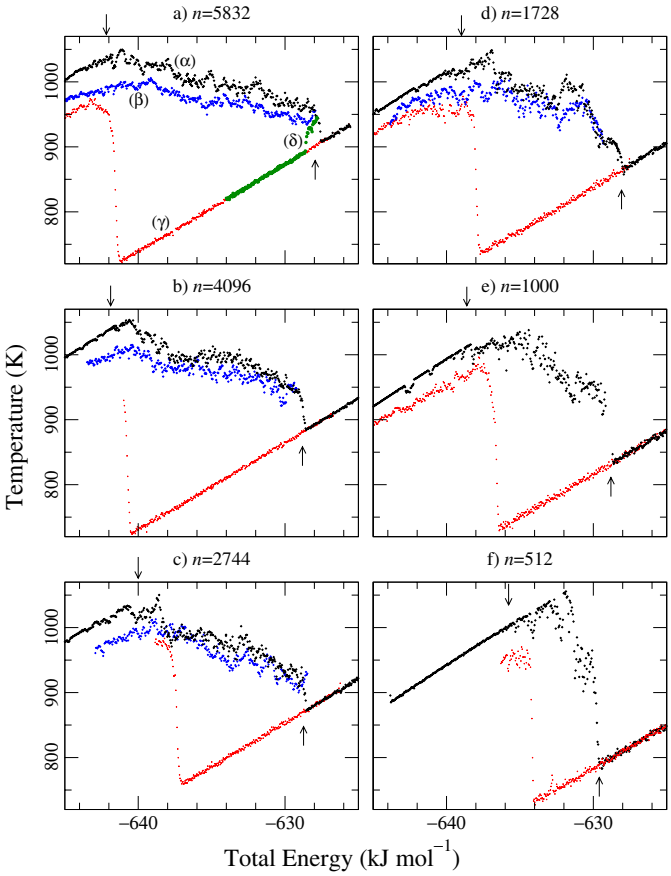

Fig. 1. (Color online) Phase change diagrams of KCl clusters. Heating is in black (α), nucleated cooling is in blue (β), non nucleated cooling is in red (γ), cooling with ineffective residual crystallite is in green (δ). Melting onset ($\downarrow$), melting end ($\uparrow$).

3 Melting

The main trends of the melting have already been reported and discussed elsewhere [41,45]. Nonetheless, we present here some improved results and details which are important for the analysis of the freezing process.

The black curves in Figure 1 show the melting behaviour for KCl clusters of different sizes by slow heating the solid. All the clusters present first-order phase transitions for which the estimated limit points for prevalence of the uniform solid are at temperatures/energies given in Table 1 (see also the arrows in Fig. 1). As expected, the melting temperatures approach the experimental bulk value as the size of the clusters increases. For clusters whose sizes are over 512 ions the melting proceeds with the presence of phase coexistence in a single aggregate in a progressively large extent, approaching a phase change at constant temperature as the size increases. At the end of melting there is a complete breakdown of the crystal and the curves follow the usual liquid-like behaviour.

It should be emphasized that since the simulations are performed by fixing the total energy, this property is, in general, the natural x-coordinate for the graphical representation of the results. The correspondence between total

Table 1. Melting points (T_m/K) for KCl clusters. Experimental bulk values are presented for comparison. Total energies (E_{tot}/kJ mol^{-1}) are also presented.

N° of ions	T_m	E_{tot}
512	∼1000	∼–636
1000	1008	–638.66
1728	1040	–639.12
2744	1046	–640.13
4096	1037	–641.84
5832	1049	–642.27
exp. [59]	1045	–
exp. [60]	1044	–

Table 2. Enthalpies of melting for clusters of different sizes (Δh/kJ mol^{-1}).

N° of ions	Δh
512	22.73
1000	23.13
1728	24.06
2744	24.24
4096	24.81
5832	25.04
exp. [61,60]	26.4
exp. [62]	25.5
exp. [63]	26.5

Table 3. Heat capacities (C_p/J K^{-1}mol^{-1}) for solid and liquid clusters of different sizes at 940 K and 1045 K. Experimental bulk values are presented for comparison.

	Solid		Liquid	
N° of ions	940 K	1045 K	940 K	1045 K
512	67.9	–	72.3	69.2
1000	68.2	–	69.6	64.7
1728	66.5	–	72.7	71.6
2744	66.4	–	71.3	68.4
4096	65.6	71.9	72.4	70.7
5832	63.6	66.2	72.0	70.0
10648			71.6	69.1
from [53]	–	64.9		
exp. [53]	–	66.9		
exp. [61,60]	64.4	69.3		73.6

energy and temperature can always be accessed, however, from Figure 1 and Tables 1, 3 and 4.

Figure 2, displays snapshots of the 4096 ions cluster at the onset and the final stage of the melting showing evidence of sustained solid-liquid coexistence. It should be noticed that for cluster sizes over ∼1000 ions the solid and liquid phases are simultaneously present and dynamically sustained in a single cluster. By slowly transferring energy to or from the system there is a reversible move along the solid-liquid coexistence. This indicates that the cluster is equilibrated. Despite the molar fractions oscillate there are no dynamical "jumps" between uniform solid and liquid forms. Moreover, dynamical alternation between melted corners of the cluster lattices is observed as much as the simulations evolve in time. It is interesting to note that the

Table 4. Self diffusion coefficients for clusters of different sizes just before spontaneous crystallization. Energies in kJ mol^{-1}, temperatures in K and self diffusion coefficients in 10^5 cm^2 s^{-1}.

N° of ions	Energy	T	SDC
1728	–637.68	734	2.90
2744	–636.86	760	3.26
4096	–640.33	726	2.73
5832	–640.82	728	2.74
10648	–641.27	735	2.71

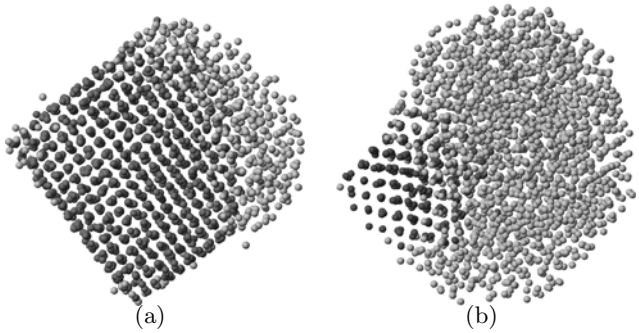

Fig. 2. Phase coexistence during the melting of the 4096 KCl cluster (a) at the onset (b) at the end.

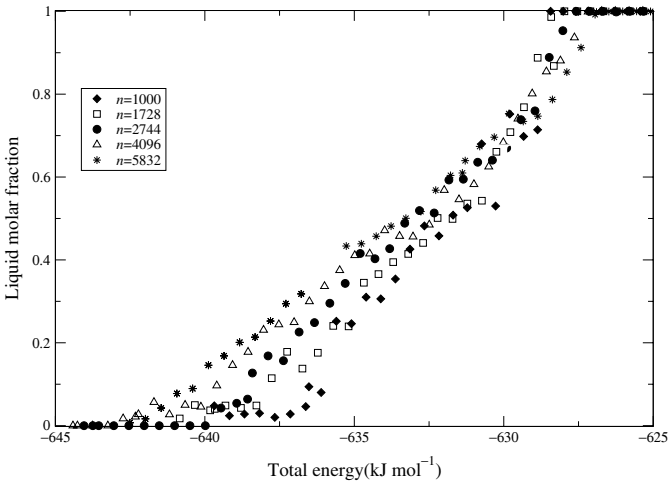

Fig. 3. Liquid molar fractions along the melting for clusters of different sizes (n).

snapshots confirm the well-known fact that alkali halides are non-self-wetting materials [42].

Using a method based on the velocity auto-correlation functions of the ions, reported elsewhere [45], it is possible to estimate the molar fraction of the liquid in the coexistence regions as a function of energy (see Fig. 3). We shall return to this function ahead.

Table 2 contains the enthalpies of melting and Table 3 presents the heat capacities before and after melting calculated from the temperature/energy curves. These results also approach the experimental bulk values and the heat capacities increase from the solid to the liquid phases.

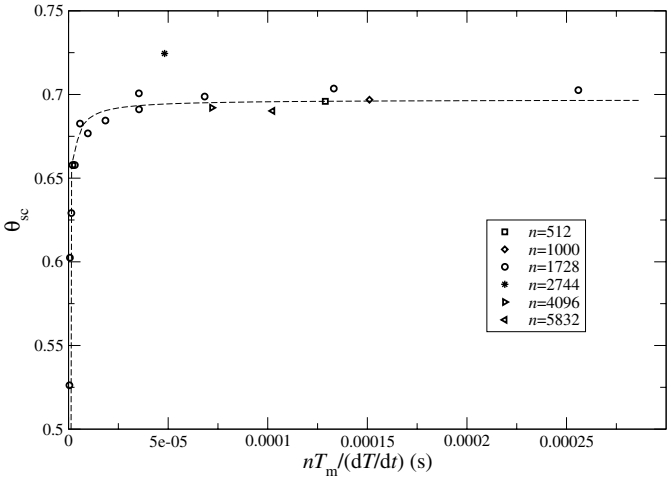

Fig. 4. θ_{sc} as a function of $nT_m/(dT/dt)$. The dashed curve is a guide for the eye.

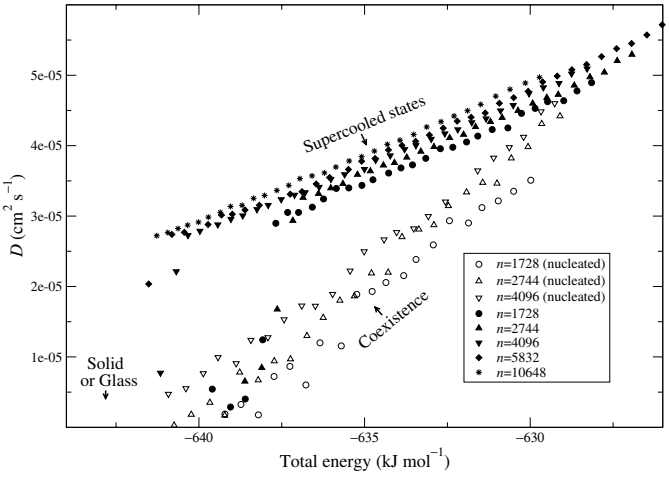

Fig. 5. Diffusion coefficients with (nucleated) and without residual crystallites.

4 Freezing

Figure 1, also displays the freezing curves obtained from totally melted configurations or from configurations not completely melted containing residual crystallites by slowly cooling the systems. The freezing process from supercooled liquid configurations plus a solid seed is displayed in separate diagrams.

4.1 Spontaneous nucleation

The diagrams of Figure 1 indicate that hysteresis cycles show up when the freezing process is carried out from totally melted configurations since spontaneous crystallization occurs at lower temperatures/energies than the ones corresponding to the complete crystal breakdown in the melting (see black and red curves). The temperature at which spontaneous crystallization occurs is, approximately, the same (∼730 K) for cluster sizes over 512. It may be suggested that this temperature (T_{sc}) corresponds to the supercooling limit of the liquid clusters according to the following analysis.

Assuming homogeneous nucleation, at least one critical nucleus must be formed in a liquid droplet of volume V so that crystallization occurs. Then, the attainable limit of supercooling for the liquid droplet, that is, the homogeneous nucleation reduced temperature $\theta_{sc} = T_{sc}/T_m$, is [64]:

$$1 = \frac{VT_m}{dT/dt}\int_1^{\theta_{sc}} J(\theta)d\theta \qquad (2)$$

where T_m is the equilibrium freezing temperature, dT/dt is the cooling rate and J is the rate of homogeneous nucleation i.e. the number of critical nucleus per unit volume and unit time.

Figure 4 shows θ_{sc} as a function of $nT_m/(dT/dt)$ computed from the previous data. The overall profile of the curve is, within the margin of statistical errors, in close agreement with the predictions of the classical nucleation theory, with the exception (also detectable in Figs. 1 and 5, and Tab. 4) of the 2744 ions cluster case which represents a fortuitous event of premature nucleation. The experimental attainable limit of supercooling for KCl is 0.836 (874 K) [64] while the average value of the plateau in Figure 4 is 0.697 (731 K). This is consistent with the fact that the sizes of our clusters are of the order of 1 nm (compared to typical droplet sizes of 1 μm in cloud chambers and 10 μm in emulsions) and the cooling rates in the simulations are considerably higher than the experimental ones. A larger amount of data with improved statistics is being produced to allow the computation of the rate of homogeneous nucleation as a function of θ and cluster size. This will presumably shed light on the time scale one can expect the critical nuclei to appear as a function of both temperature and cluster size.

Although vitrification is possible to occur in simulated clusters or bulk KCl, by applying instantaneous or very high cooling rates [65,41], it appears that the present simulations have prevented it. In fact, it has been detected that such systems present a glass transition at $\theta \sim 0.3$ (∼300 K). The temperatures in the present simulation are above this value. From Figure 4 it can also be inferred that the probed conditions (cooling ratios and cluster sizes) are above (though not too far) the region where vitrification is concurrent with crystallization. Moreover, the self-diffusion coefficients in the supercooled region show a liquid behaviour and have higher values than the ones of coexistent states (see Fig. 5).

Figure 6 represents the liquid molar fractions obtained during the cooling with and without residual crystallites. The inset is a zoom of the supercooled liquid molar fractions. It is clear that the supercooled liquid, obtained from totally melted states, contains traces of solid-like ions. However, they do not form a single solid (pre-critical) nucleus inside the liquid droplet. On the contrary, they constitute sparse clouds of individual ions trapped by their neighbours (with lifetimes $\gtrsim$40 ps) whose percentage increases as the temperature decreases. Figure 7 displays the fraction of solid-like ions as a function of temperature

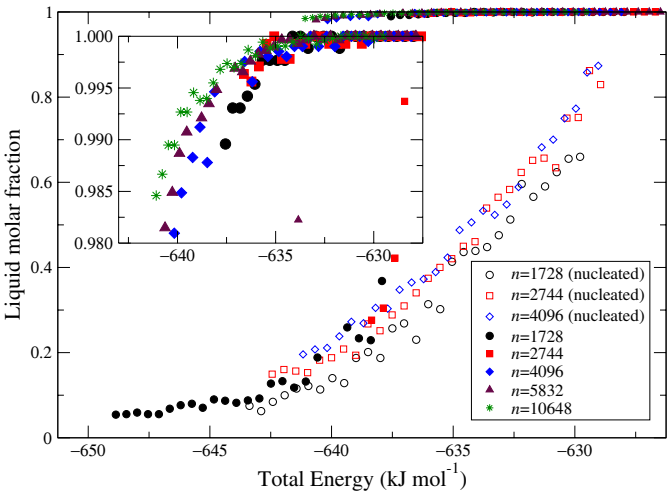

Fig. 6. (Color online) Liquid molar fractions along the cooling with (nucleated) and without residual crystallites for clusters of different sizes (n).

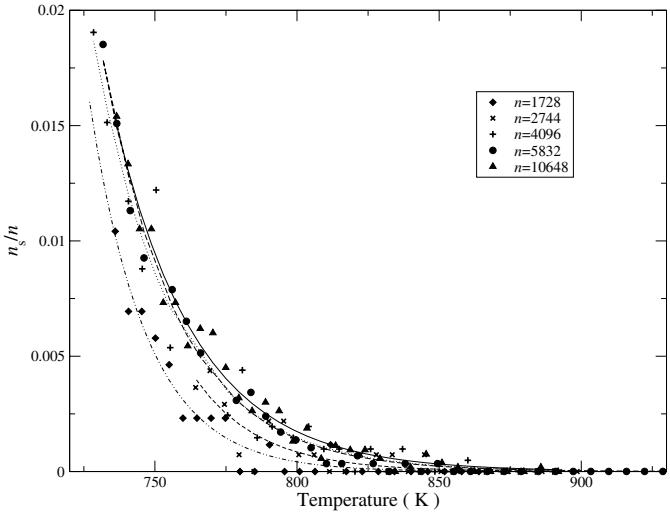

Fig. 7. Fraction of solid-like ions, in the supercooled liquid, as a function of temperature for clusters of different sizes (n).

and Table 5 the fitting coefficients to:

$$\frac{n_{\rm s}}{n} = C \exp\left[\gamma\,(T - T_0)\right] \qquad (3)$$

where $n_{\rm s}$ and n are the number of solid-behaved ions and the total number of ions respectively. The curves have a steep increase at ∼730 K. The fitting coefficients seem to be uncorrelated with the size of the clusters and for the bigger ones the curves almost coincide. Considering that the probability of spontaneous nucleation increases with the fraction of solid-like ions in the supercooled liquid the exponential form seems to describe the homogeneous nucleation process in the present clusters.

4.2 Heterogeneous nucleation

As for the freezing process starting at configurations not completely melted containing residual crystallites, the behaviour is clearly different (see blue curves in Fig. 1) since the liquid already contains nucleus which mimic the seeds in heterogeneous nucleation. The hysteresis practically disappears and the freezing curves approach the melting ones. However, if the liquid is not sufficiently nucleated, then supercooling and hysteresis show up again (see green curve in Fig. 1).

The last observations called for a further analysis of heterogeneous nucleation by means of introducing external seeds as small crystallites that collide with the liquid droplet. In this way one can assess the critical nucleus sizes for an effective nucleation. We have firstly chosen a set of configurations at different energies of the 5832-ion cluster, in the supercooled liquid branch, and extracted 512 ions from them. After the thermal stabilization of the resulting liquid droplets we have added one seed (a solid crystallite with 512 ions) in the neighbourhood of the droplets (see Fig. 8) and then followed the seeded droplets time evolution which is displayed in Figure 9.

Table 5. Values of the exponent factor γ (in K^{-1}), and prefactor C obtained from the fittings to equation (3).

n° of ions	γ	C
1728	–0.038	0.011
2744	–0.026	0.008
4096	–0.031	0.017
5832	–0.038	0.022
10648	–0.033	0.020

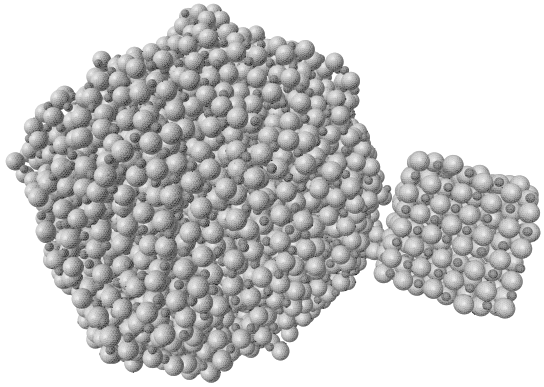

Fig. 8. Snapshot of the liquid droplet (n = 5832–512) in the presence of a small crystal seed (n = 512).

4.2.1 Phenomenological analysis of the crystal growth dynamics

The general evolution shows that the temperature increases rapidly with time when the energy is relatively low, until it reaches the solid or the coexistence solid-liquid curves. From there on the temperature stabilizes along the time. The noticeable gap near the middle of the energy axes is due to the shorter runs performed at these state points. The rate of temperature variation decreases as the energy increases and from a value of energy ~ -630 kJ mol^{-1} upwards the temperature ceases to

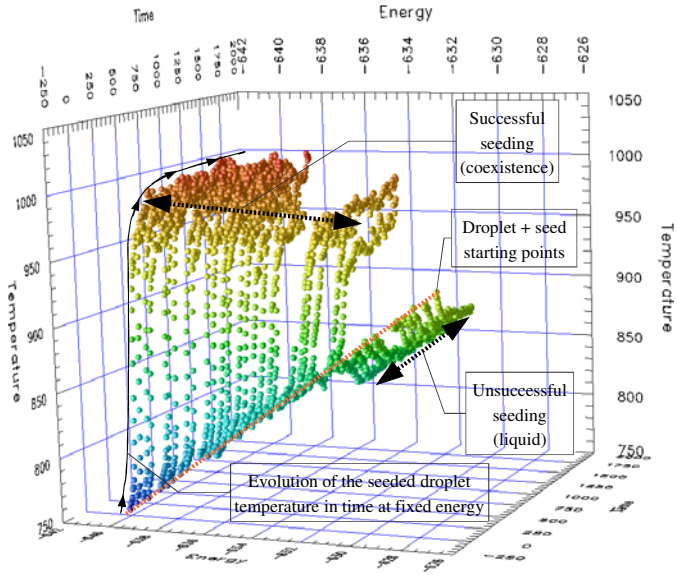

Fig. 9. (Color online) Induced crystal growth dynamics (temperature evolution in time at fixed energy) of a supercooled liquid droplet ($n = 5832$–512) ions, using a seed of 512 ions. Bullets are coloured according to the system temperatures ranging from blue (for the lowest ones) to red (for the highest ones). Time in ps, temperature in K and total energy in kJ mol^{-1}.

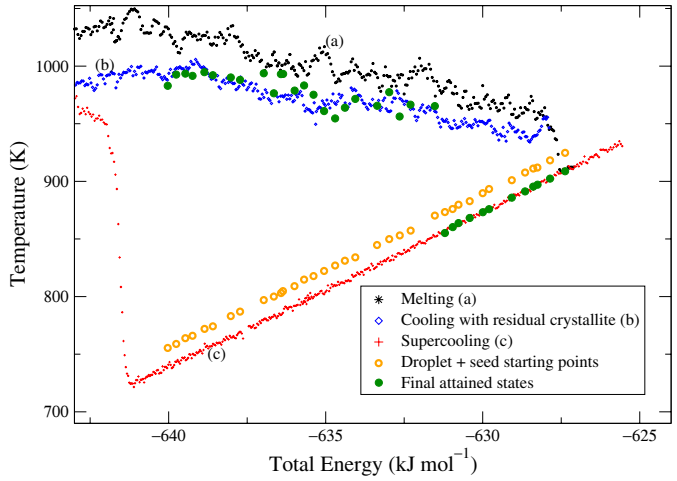

Fig. 10. (Color online) Temperatures of the starting and final states attained by the seeded droplets. Supercooled liquid and phase coexistence are also represented for comparison.

increase and the system reaches the same supercooled states obtained by cooling the non-nucleated liquid droplet. This is better illustrated in Figure 10 to which we shall return ahead.

Figure 11 shows an example of the temperature evolution with time of the liquid droplet and solid crystallite. Note that the solid seed has, at the outset, the temperature ∼975 K, the supercooled liquid droplet (5832–512 ions) the temperature ∼755 K and the resulting seeded droplet the temperature ∼775 K (corresponding to the energy of ~ -639 kJ mol^{-1}). For this proportion between seed (512 ions) and droplet (5832–512 ions)

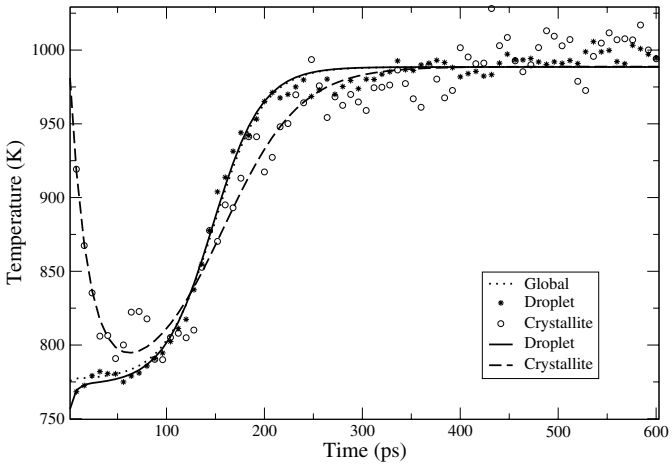

Fig. 11. Temperature evolution for liquid droplet and seed.

sizes, the seeded droplet (5832 ions) temperature is always about 20 K higher than the unseeded droplet (5832 ions) temperature corresponding to the same energy, as illustrated in Figures 9 and 10, independently of the initial states of the sub-aggregates. The simulation results have been fitted to the equation:

$$T = a_0 + a_1 \mathrm{e}^{a_2 t} + \frac{a_3}{1 + \mathrm{e}^{a_4 (t - a_5)}}. \quad (4)$$

The exponential term accounts for the temperature time evolution of each sub-aggregate until the onset of contact and thermal equilibrium between them. The sigmoid term accounts for the rest of the process. The constant a_0 is, on average, the equilibrium temperature of the droplet plus seed at contact.

The fittings suggest the definition of three time periods. The period to establish the contact between the liquid droplet and the solid seed as the elapsed time from the start of the simulation to the instant where the exponential fitted to the crystallite data reaches a value ∼0.1. The induction period as the elapsed time from the instant of contact to the point where the sigmoid fitted to the global temperature of the system reaches ∼1/10 of its maximum value. From this instant until the sigmoid reaches ∼9/10 of its maximum value a period of rapid crystalline growth is observed. The three periods are discriminated for different energies in Figure 12. The induction periods in the energy interval -634 kJ mol^{-1} (819 K) to -631 kJ mol^{-1} (859 K) have a noticeable increase preceding the point where the seed looses efficiency to induce order in its neighbourhood. Figures 9 and 10 confirm that below -630 kJ mol^{-1} and 855 K the seed is efficient inducing a solid or a phase coexistence after short time intervals. Figure 13 shows a snapshot obtained from a seeded liquid droplet at -641 kJ mol^{-1} after ∼1 ns. It is a crystal though imperfect.

These results indicate that phase coexistence is stable (and sustained during the lifetime of the clusters) relatively to the supercooled liquid at the same energies, up to nearly the point where the final breakdown of the crystal takes place on melting.

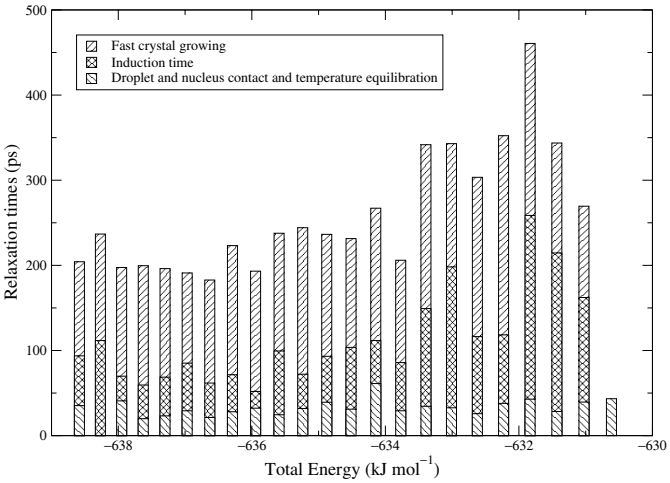

Fig. 12. Relaxation times of contact and temperature equilibration, induction and crystal growth.

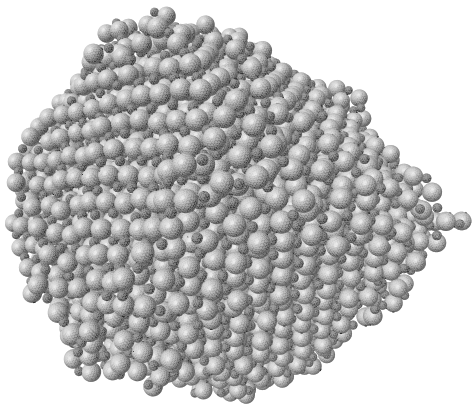

Fig. 13. A snapshot of a solid cluster, after 1.376 ns, obtained by seeding a liquid droplet.

4.2.2 Seed effectiveness limit

The effectiveness of seeding is a well-known question discussed in the literature [64] and involving theoretical models and experimental data. To our knowledge, however, there is a lack of simulation results in particular for alkali halide nanoclusters at temperatures near the melting point. We have also performed simulations starting with the same supercooled liquid droplet of 5832 ions and using smaller seeds with 64 and 216 ions. In these cases the liquid droplets have approximately the same size as for the 512-ion seed (5832–64 and 5832–216 ions respectively).

In the case of the 64 ions crystallite, the seed is ineffective in all the existence range of the probed supercooled liquid, even for values of energy/temperature near the occurrence of spontaneous nucleation (∼730 K).

As for the case of the 216 ions crystallite, the seed is effective, but only in a shorter range of temperature/energy than in the case of the 512 ions seed. Above 785 K the seed looses its efficiency. However, below that temperature the behaviour of the system, namely its time evolution periods, is similar to the 512 case. Thus, it seems that the difference between the results obtained with seeds of different sizes is only in the temperature below which the seed is effective.

4.3 Sizes of critical nuclei

In order to assess the consistency of the simulation results we have used a theoretical model to predict the size of the critical nucleus, that is, the minimum size of the seed that is effective at a given temperature T.

For spherical seeds and homogeneous nucleation the radius of the critical nucleus, r^*, is given by Debenedetti [64]:

$$r^* = \frac{2\sigma\upsilon T_\mathrm{m}}{(T_\mathrm{m} - T)\Delta h} \tag{5}$$

where σ is the surface tension in the interface, υ is the specific volume of the solid, T_m is the equilibrium crystallization temperature and Δh is the enthalpy of melting.

For cubic seeds, we can derive a similar equation for the edge of the critical cube:

$$l^* = \frac{4\sigma\upsilon T_\mathrm{m}}{(T_\mathrm{m} - T)\Delta h}. \tag{6}$$

The average number of particles by one edge of the cube, n_a^*, is:

$$n_\mathrm{a}^* = \frac{4\upsilon^{\frac{2}{3}}\sigma T_\mathrm{m}}{(T_\mathrm{m} - T)\Delta h} \tag{7}$$

and multiplying both members by $\upsilon^{1/3}$, equation (6) is obtained.

As we are mainly interested in checking out the consistency of the simulation results we have proceeded as follows. Assuming that σ and υ are independent on the temperature [64], the last equation can be rewritten in the form:

$$\frac{n_\mathrm{a}^*(T_\mathrm{m} - T)}{T_\mathrm{m}} = k. \tag{8}$$

In the case of the 512 ions seed, $n_\mathrm{a}^* = 8$, $T_\mathrm{m} = 1049$ K and $T = 855$ K. Therefore, the value of k is 1.48 and the highest temperature at which other seeds are effective should be given by:

$$T = T_\mathrm{m} - k\frac{T_\mathrm{m}}{n_\mathrm{a}^*}. \tag{9}$$

For the 216 ions seed the predicted temperature is 790 K in good agreement with the simulation value of 785 K. In the case of the 64 ions seed the predicted temperature is 661 K well below the temperature of spontaneous crystallization, and in accordance with the systematic destruction of the seed observed along the probed supercooled region.

Using $k = 1.48$ the estimated solid-liquid interfacial tension is $\sigma = 154$ mJ m^{-2}. The value for the

Table 6. Critical nuclei sizes n_s as a function of the temperature (T/K). (a) Values collected from the size of residual crystallites. The number of the ions of the clusters from where the data was collected are presented between parenthesis. (b) Values obtained from the seeding process.

n_s	T			
	(a)		(b)	
216			785	(5832)
512			855	(5832)
290	875	(1000)		
328	893	(1728)		
630	922	(2744)		
634	905	(4096)		
874	939	(5832)		

bulk solid-gas interface, calculated by Fietcher [66], is $\sigma_s = 168\ \mathrm{mJ\,m^{-2}}$. For the bulk liquid-gas interface $\sigma_l = 97.83\ \mathrm{mJ\,m^{-2}}$, experimentally measured by Sato et al. [67]. From the Antonov rule [68] $\sigma = \sigma_s - \sigma_l = 70.2\ \mathrm{mJ\,m^{-2}}$ was expected. So, the actual prediction, while of the same order of magnitude, overestimates the bulk value.

We should point out that, apart from the assumption of σ and v being independent on the temperature, the application of equation (7) to the present cases does not strictly obey to the conditions of its derivation. Indeed, the equation is obtained supposing homogeneous nucleation where the spontaneous critical nucleus is well inside the liquid, that is, completely wetted. It is well-known, however, that alkali halides are non-self-wetting materials as we have referred to before. Consequently, the seeds remain outside the liquid droplet during the crucial steps of the crystal growth process with their faces not completely wetted. Moreover, the equation presupposes a bulk liquid phase which is not exactly the case. Even so the results appear to be consistent.

We have also estimated the size of the critical nucleus for the freezing process starting at configurations not completely melted containing residual crystallites, by analysing the solid portion of the cluster remaining at the final stage of the melting process. The maximum energy where the residual crystallite constitutes an effective nucleus is taken from the crossing point of the melting and recrystallization curves (black and blue curves in Fig. 1). The size of the crystallite is then estimated by interpolation of the liquid molar fractions in Figure 3. Table 6 contains the results for clusters of different sizes together with the ones for heterogeneous nucleation. Figure 14 displays the inverse of the average number of particles by one edge of the cubic nucleus as a function of temperature. Note that the straight line approach 0 as $T \to T_m$ according to equation (7). Considering that the method used to compute the results referring to residual crystallites is a bit crude and that, in the two sets of results, the nuclei are differently wetted it seems that there is a fairly good regular behaviour.

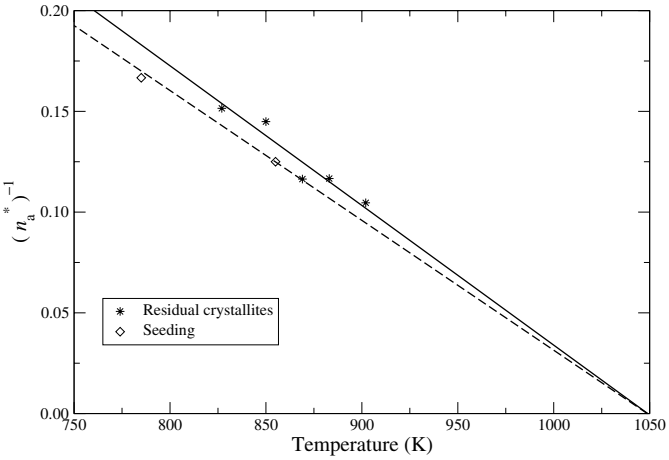

Fig. 14. Inverse of the average number of particles by one edge of the cubic nucleus as a function of temperature. Diamonds represent data extracted from seeding, stars represent data obtained from residual crystallites.

5 Concluding remarks

We have shown and discussed some relevant aspects of the melting, freezing and nucleation in unconstrained clusters of potassium chloride. Whenever possible the simulation results have been compared with available experimental data.

We should point out that once the simulated clusters are unconstrained (at virtually zero pressure) a true thermodynamic equilibrium is never attained. Therefore, all the references to solid, liquid and coexistent phases should be understood as metastable states whose life time is longer than the observation time which, in the present simulations, is of the order of 10^2 ns.

The present study needs to be complemented by a full theoretical analysis of the simulation results to further correlate and predict the whole set of data. Indeed, a proper discussion on stability demands, for example, the consideration of free-energies which have not been analysed in the present article. Vitrification is also a possible outcome of supercooling, well suited to be probed by molecular dynamics. These and other aspects, such as the existence of different solid phases in clusters of LiCl, will be reported in forthcoming papers.

One of us (P. Rodrigues) gratefully acknowledges the institutional support of the Department of Chemistry and Biochemistry, FCUL, during his research work. We thank Intel Corporation for the free access to their compilers and the GNU and Linux communities for all the invaluable tools they offer.

References

1. D.J. McGinty, J. Chem. Phys. **58**, 4733 (1973)
2. C.L. Briant, J.J. Burton, J. Chem. Phys. **63**, 2045 (1975)
3. M. Amini, D. Fincham, R.W. Hockney, J. Phys. C: Solid St. Phys. **12**, 4707 (1979)

4. N. Quirke, Mol. Simul. **1**, 249 (1988)
5. R.B. McClurg, J. Aerosol Sci. **29**, S43 (1998)
6. S. Sugano, H. Koizumi, *Microcluster Physics* (Springer, 1998)
7. F.S. Zhang, E. Suraud, F. Calvo, F. Spiegelmann, Chem. Phys. Lett. **300**, 595 (1999)
8. D.J. Wales, R.S. Berry, J. Chem. Phys. **92**, 4473 (1990)
9. R.S. Berry, B.M. Smirnov, J. Chem. Phys. **114**, 6816 (2001)
10. J.P.K. Doye, D.J. Wales, W. Branz, F. Calvo, Phys. Rev. B **64**, 1 (2001)
11. R.S. Berry, C. R. Phys. **3**, 319 (2002)
12. M. Ma, W. Lu, J. Huang, J. Solid State Chem. **165**, 289 (2002)
13. S.P. Huang, P.B. Balbuena, J. Phys. Chem. B **106**, 7225 (2002)
14. J. Huang, L.S. Bartell, J. Phys. Chem. A **106**, 2404 (2002)
15. L.S. Bartell, J. Phys. Chem. A **106**, 10893 (2002)
16. L.S. Bartell, Y.G. Chushak, J. Huang, Atmosph. Res. **65**, 153 (2003)
17. G.W. Turner, Y.G. Chushak, L.S. Bartell, J. Phys. Chem. A **108**, 1666 (2004)
18. R.A. Eppler, H.G. Drickamer, J. Phys. Chem. Sol. **6**, 180 (1958)
19. T. Ohta, S. Kinoshita, H. Kuroda, J. Electron. Spectrosc. Relat. Phenom. **12**, 169 (1977)
20. A. Elafif, R.C. Karnatak, J.M. Esteva, C.M. Teodorescu, M. Womes, E. Bouisset, Physica B **208&209**, 115 (1985)
21. R.N. Barnett, C.L. Cleveland, H. Häkkinen, W.D. Luedtke, C. Yannouleas, U. Landman, Eur. Phys. J. D **9**, 95 (1999)
22. V. Pennanen, M. Huttula, H. Aksela, E. Nommiste, S. Aksela, J. Electron. Spectrosc. Relat. Phenom. **114–116**, 169 (2000)
23. M.A. Gaveau, M. Briant, P.R. Fournier, J.M. Mestdagh, J.P. Visticot, F. Calvo, S. Baudrand, F. Spiegelman, Eur. Phys. J. D **1**, 153 (2002)
24. G. Ehrlich, Surf. Sci. **299**, 628 (1994)
25. S. Uda, J. Cryst. Growth **140**, 128 (1994)
26. J.W. Hovick, L.S. Barrell, J. Mol. Struct. **413**, 615 (1997)
27. J. Urban, Cryst. Res. Technol. **33**, 1009 (1998)
28. K.A. Jackson, Ind. Eng. Chem. **57**, 28 (1965)
29. H. Reiss, J. Stat. Phys. **2**, 83 (1970)
30. J.W.P. Schmelzer, J. Coll. Interf. Sci. **242**, 354 (2001)
31. M. Amini, R.W. Hockney, J. Non Cryst. Sol. **31**, 447 (1979)
32. M. Amini, D. Fincham, R.W. Hockney, J. Phys. C: Sol. St. Phys. **13**, L221 (1980)
33. J. Jellineck, T.L. Beck, R.S. Berry, J. Chem. Phys. **84**, 2783 (1986)
34. T.L. Beck, R.S. Berry, J. Chem. Phys. **88**, 3910 (1988)
35. D.M.L. Thomas, L. Beck, R.S. Berry, J. Chem. Phys. **89**, 1681 (1988)
36. D.J. Wales, R.S. Berry, J. Chem. Phys. **92**, 4295 (1990)
37. Y. Sakamoto, J. Phys. Soc. Jap. **59**, 3925 (1990)
38. J.P. Rose, R.S. Berry, J. Chem. Phys. **96**, 517 (1992)
39. J.P. Rose, R.S. Berry, J. Chem. Phys. **98**, 3246 (1993)
40. J.P. Rose, R.S. Berry, J. Chem. Phys. **98**, 3262 (1993)
41. F.M.S.S. Fernandes, L.A.T.P. Neves, Am. Inst. Phys. Conf. Proc. **330**, 313 (1995)
42. C.L. Cleveland, U. Landman, W.D. Luedtke, J. Phys. Chem. **98**, 6272 (1994)
43. F. Calvo, P. Labastie, J. Phys. Chem. B **102**, 2051 (1998)
44. F.M.S. Fernandes, P.C.R. Rodrigues (1998), `http://elixir.dqb.fc.ul.pt`
45. P.C.R. Rodrigues, F.M.S.S. Fernandes, Int. J. Quant. Chem. **84**, 169 (2001)
46. A. Proykova, S. Pisov, R.S. Berry, J. Chem. Phys. **115**, 8538 (2001)
47. F. Despa, R.S. Berry, Eur. Phys. J. D **16**, 261 (2001)
48. A. Proykova, D. Nikolova, R.S. Berry, Phys. Rev. B **65**, 085411 (2002)
49. P.C.R. Rodrigues, F.M.S.S. Fernandes, Eur. Phys. J. D (submitted)
50. R.O. Watts, I.J. McGee, *Liquid State Chemical Physics* (John Wiley and Sons, 1976), pp. 307–312
51. M.P. Allen, D.J. Tildesley, *Computer Simulation of Liquids* (Claredon Press, Oxford, UK, 1987)
52. L.V. Woodcock, Chem. Phys. Lett. **10**, 257 (1970)
53. L.V. Woodcock, K. Singer, Trans. Faraday Soc. **67**, 12 (1971)
54. M.J.L. Sangster, M. Dixon, Adv. Phys. **25**, 247 (1976)
55. F.J.A.L. Cruz, J.N.C. Lopes, J.C.G. Calado, M.E.M. da Piedade, J. Phys. Chem. B **109**, 24473 (2005)
56. F.J.A.L. Cruz, J.N.C. Lopes, J.C.G. Calado, J. Phys. Chem. B **110**, 4387 (2006)
57. F.J.A.L. Cruz, J.N.C. Lopes, J.C.G. Calado, Fluid Phase Equilib. **241**, 51 (2006)
58. K. Huang, *Statistical Mechanics* (John Wiley and Sons, New York, 1987)
59. E.R. Buckle, A.R. Ubbelohde, Proc. Roy. Soc. A. **259**, 325 (1960)
60. *NIST Chemistry WebBook, NIST Standard Reference Database Number 69*, edited by P.J. Linstrom, W.G. Mallar (National Institute of Standards and Technology, Gaithersburg MD, 20899, 2003), `http://webbook.nist.gov`
61. J.M.W. Chase, J. Phys. Chem. Ref. Data, Monograph 9 **27**, I (1998), `http://webbook.nist.gov`
62. S. Rice, W. Klemperer, J. Chem. Phys. **27**, 643 (1957)
63. A.S. Dworkin, M.A. Bredig, J. Phys. Chem. **64**, 269 (1960)
64. P.G. Debenedetti, *Metastable Liquids, Concepts and Principles* (Princeton University Press, New Jersey, 1996)
65. L.V. Woodcock, C.A. Angell, P. Cheeseman, J. Chem. Phys. **65**, 1565 (1976)
66. S. Fiechter, Sol. Energy Mater. Sol. Cells **83**, 459 (2004)
67. Y. Sato, T. Ejima, M. Fukasawa, K. Abe, J. Phys. Chem. **94**, 1991 (1990)
68. Y.G. Chushak, L.S. Bartell, J. Phys. Chem. B **105**, 11605 (2001)